Rapid Communications

Measurement-induced randomness and structure in controlled qubit processes

Ariadna E. Venegas-Li,[*] Alexandra M. Jurgens,[†] and James P. Crutchfield[‡]
Complexity Sciences Center and Physics Department, University of California at Davis, One Shields Avenue, Davis, California 95616, USA

(Received 23 August 2019; revised 30 December 2019; accepted 14 September 2020; published 6 October 2020)

When an experimentalist measures a time series of qubits, the outcomes constitute a classical stochastic process. We show that projective measurement induces high complexity in these processes in two specific senses: They are inherently random (finite Shannon entropy rate) and they require infinite memory for optimal prediction (divergent statistical complexity). We identify nonorthogonality of the quantum states as the mechanism underlying the resulting complexities and examine the influence that measurement choice has on the randomness and structure of measured qubit processes. We introduce quantitative measures of this complexity and provide efficient algorithms for their estimation.

DOI: 10.1103/PhysRevE.102.040102

Introduction. Temporal sequences of controlled quantum states are key to fundamental physics and its engineering deployment. Quantum entanglement [1] between emitted qubits, such as photons [2], is central to Bell probes [3] of inconsistencies between quantum mechanics and local hidden variable theories [4]. Complementing their scientific role, entangled qubits are now recognized as basic resources for quantum technologies—quantum key distribution [5], teleportation [6], metrology [7], and computing [8]. The quest there is for qubit sources that allow *on-demand* generation: At a certain time a source should emit one and only one pair of entangled photons. Qubit sources should also be *efficient*: qubits emitted and collected with a high success rate. Also, individual qubits should have *specified properties*. In Einstein-Podolsky-Rosen (EPR) experiments photons in emitted pairs should be identical from trial to trial. In addition, in communication systems polarization states should be manipulable at the highest possible rates [9].

Much experimental effort has been invested to develop qubit sources that, for example, extract entangled photons from trapped atoms [10,11], spontaneous parametric down-conversion [12], quantum dots [13], and related circuit-QED (CQED) systems [14]. To date, though, there is still no single-qubit source that exactly meets the performance requirements. The on-demand criterion has been particularly vexing [15]. Addressing these challenges leads rather directly to a common question, one that touches on both fundamental physics and quantum engineering: *how to characterize the statistical and structural properties of a qubit time series.* The underlying challenge is that a systematic description of quantum processes with memory in terms of experimental measurements has yet to be given [16].

Complementing this, techniques developed within quantum process tomography and process reconstruction [17–23] achieve partial or total reconstruction of channels and system evolution. This task is of particular importance with the advent of physically realizing processing in multiqubit systems; notably, some are now available as open cloud services [24,25]. This progress only heightens the need to fully characterize quantum process information and statistics. In the domain of classical stochastic processes, these properties determine simulation capabilities, memory requirements, and predictability, and they quantify a process' randomness and structure [26,27].

To address these challenges we concern ourselves with a source that generates a single qubit at a time. We imagine that the on-demand source is used repeatedly, producing an arbitrarily long time series, which we call a *qubit process*. A simple example arises when monitoring sequential emissions from a blinking quantum dot [28,29]. We refer to their generators as *controlled qubit sources* (CQSs). We ask how random and structured they appear to an experimentalist. [Supplemental Material (SM) [30] Sec. I highlights the features of the quantum formalism we use.]

Here, we introduce a qubit source that is classically controlled and quantally measured—for short, a *classically controlled qubit source* (cCQS). While controllers take many forms, the following models them as hidden Markov models (HMMs)—a standard representation of stochastic discrete-state controllers. Finite-state HMMs generate finite-memory processes and come with tools for quantifying their essential informational and statistical properties. They are also widely used as models of noisy classical sources and communication channels [31–33]. (See SM [30] Sec. II A for a refresher on HMMs.) The qubit generator proper is sandwiched between the controller and measurement apparatus. Figure 1 (top) illustrates the setup: A black box, representing a quantum system, emits a qubit in quantum state ρ_t at each time t. More concretely, the lower panel shows an example, revealing that the controller inside the black box is a finite-state hidden Markov model that emits qubits in various quantum states.

We restrict the qubit states emitted by the cCQS to be pure-state density matrices, that is, $\rho_t^2 = \rho_t$. This limits the

[*]avenegasli@ucdavis.edu
[†]amjurgens@ucdavis.edu
[‡]chaos@ucdavis.edu

 ©2020 American Physical Society

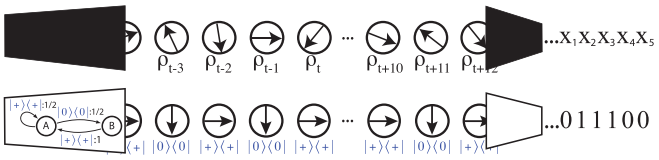

FIG. 1. Top: A general controlled qubit source (CQS) as a discrete-time quantum dynamical system that generates a time series of qubits $\rho_{t-2}\rho_{t-1}\rho_t \ldots$. Bottom: A cCQS generates a qubit process $|0\rangle\langle 0|, |+\rangle\langle +| \cdots$. Measuring each qubit, an observer sees a classical stochastic process: $\ldots x_1x_2x_3x_4x_5$ (top), $\ldots 011100$ (bottom).

type of correlations that can be present across the qubit time series to classical correlations and leaves time series with temporal entanglement for future exploration. The quantum state of the random variable chain that forms the time series can be regarded as the tensor product of the individual qubits: $\cdots \rho_{t-2} \otimes \rho_{t-1} \otimes \rho_t \cdots$.

This simple setup raises several natural questions about characterizing qubit processes generated by CQSs. How random is the qubit process? How much memory does the source use to generate the qubit series? Can we identify the internal control mechanism from the qubit time series alone?

By way of comparison to CQSs, in the classical setting all of these questions can be answered constructively. Importantly, this setting provides a scaffolding to answer the questions for CQS-generated processes. So, let us review. In a classical system that emits symbols X taking values in a discrete alphabet ($x \in \mathcal{A}$), the output is a *stochastic process* $\Pr(X_{-\infty:0}, X_{0:\infty})$ over pasts $X_{-\infty:0}$ and futures $X_{0:\infty}$. Here, X_t denotes the random variable at time t and a block is denoted $X_{t:t+l} = X_t, X_{t+1}, \ldots, X_{t+l-1}$.

On the one hand, the process' *Shannon entropy rate* h_μ,

$$h_\mu = \lim_{\ell \to \infty} \frac{\mathrm{H}[\Pr(X_{0:\ell})]}{\ell},$$

measures its randomness as the rate of increase of information in length-ℓ sequences—in the *Shannon block entropy* $\mathrm{H}[\Pr(X_{0:\ell})]$ [34]. On the other hand, accurately determining a process' memory requires the generating HMM to have specific properties. Fortunately, there is a canonical HMM that gives a direct, closed-form expression for both properties.

This is the process' *ϵ-machine* [27]—its minimal optimally predictive HMM—and it satisfies the following. First, the ϵ-machine is *unifilar*: For each state $s_k \in \mathcal{S}$ and each symbol x there is at most one transition from s_k that emits x. Second, its states are *probabilistically distinct*: For every pair of states $s_k, s_j \in \mathcal{S}$ there exists some finite word $w = x_0x_1 \cdots x_{\ell-1}$ such that $\Pr(w|s_k) \neq \Pr(w|s_j)$. These features define a process' *causal states*, meaning they capture the minimal amount of information from the past to optimally predict the process' future. Together with their transition dynamic $\{T^{(x)} : x \in \mathcal{A}\}$ the causal states form the process' ϵ-machine. [Figures 2(a)–2(c) give examples of unifilar and nonunifilar HMMs.] Though a seemingly innocent structural property, we show that unifilarity plays a decisive role in diagnosing the complexity of measured quantum processes.

To calculate the resources required to predict future outputs, we find the *statistical complexity* C_μ—the Shannon information or average memory in the causal states,

$$C_\mu = -\sum_{s \in \mathcal{S}} \Pr(s) \log_2 \Pr(s). \tag{1}$$

Additionally, in the classical setting unifilarity allows one to calculate the entropy rate directly from the ϵ-machine as the state-averaged symbol uncertainty,

$$h_\mu = -\sum_{s \in \mathcal{S}} \Pr(s) \sum_{x \in \mathcal{A}} \sum_{s' \in \mathcal{S}} T^{(x)}_{ss'} \log T^{(x)}_{ss'}. \tag{2}$$

(See SM [30] Sec. II B.)

We can now state our main result: Even with a finite-state HMM control, *generically a cCQS produces a measured qubit process whose minimal optimal predictor requires an infinite number of causal states.*[1] Prediction resources (C_μ) diverge, though at a quantifiable rate. We establish the result constructively, by determining h_μ and exploring C_μ's divergence for qubit processes and by identifying the driving mechanism as *measurement-induced nonunifilarity*.

Qubit processes. Generating the qubits in a time series is governed by a cCQS that, without loss of generality, we take to be an ϵ-machine for which the symbols emitted during state-to-state transitions consist of qubit states. This HMM choice ensures that the source's internal complexity used in generating the qubit process can be quantified. Both the entropy rate h^g_μ and the statistical complexity C^g_μ of the controller can be exactly computed from the cCQS, since it is an ϵ-machine.

The states of the qubits' output by a cCQS form a stochastic process; two examples of the latter are shown in Figs. 2(a) and 2(b). (SM [30] Secs. I and II A explain how these qubit-generating state machines operate.) The cCQS in Fig. 2(a) generates a qubit time series of orthogonal pure states $|0\rangle\langle 0|$ and $|1\rangle\langle 1|$. The cCQS in Fig. 2(b) generates a qubit time series of nonorthogonal pure states $|0\rangle\langle 0|$ and $|+\rangle\langle +|$, where $|+\rangle = (|0\rangle + |1\rangle)/\sqrt{2}$.

Measured qubit processes. The observer interacts with such processes by applying to each qubit a projective measurement, consisting of the set of orthonormal measurement operators $\{E_0, E_1\}$ with measurement basis $E_0 = |\psi_0\rangle\langle\psi_0|$ and $E_1 = |\psi_1\rangle\langle\psi_1|$ parametrized by the Bloch angles θ and ϕ via

$$|\psi_0\rangle = \cos\frac{\theta}{2}|0\rangle + e^{i\phi}\sin\frac{\theta}{2}|1\rangle \tag{3a}$$

and

$$|\psi_1\rangle = \sin\frac{\theta}{2}|0\rangle - e^{i\phi}\cos\frac{\theta}{2}|1\rangle. \tag{3b}$$

The outcome of each measurement can then be labeled 0 or 1, respectively, resulting in a binary classical stochastic process.

Knowledge of the controller and the measurement basis allows us to directly construct an HMM that generates the measured qubit process itself. We call this the *measured* cCQS: It has the same states and stationary distribution π as the original cCQS. Its labeled transition matrices $\{T^{(x)}\}$ with

[1]Genericity here refers to any HMM that is ergodic, aperiodic, and non-negative.

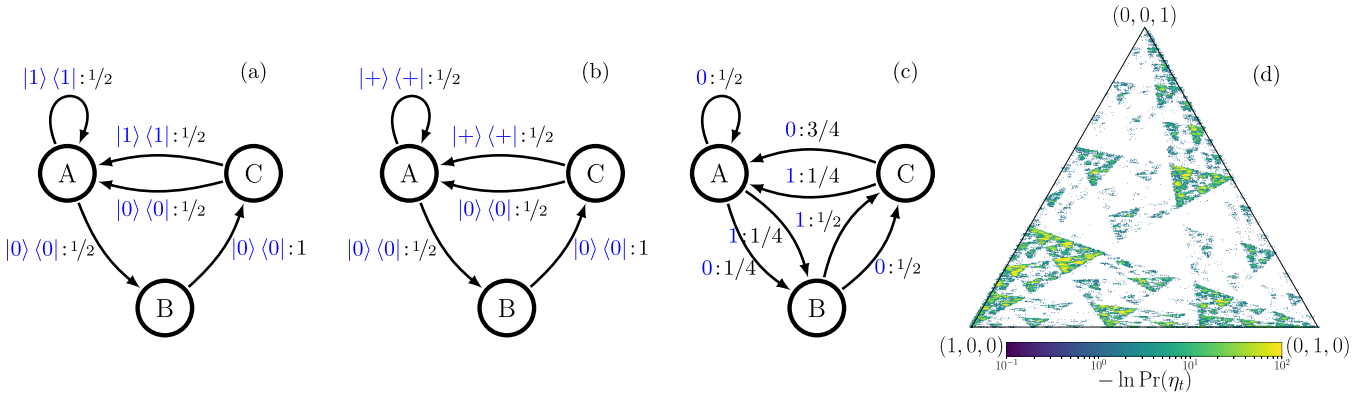

FIG. 2. (a) Three-state classically controlled qubit source (cCQS) that generates a process consisting of qubits in orthogonal states. (b) Nonorthogonal-qubit cCQS: Three-state HMM that outputs nonorthogonal pure states $|0\rangle\langle 0|$ and $|+\rangle\langle +|$, where $|+\rangle = (|0\rangle + |1\rangle)/\sqrt{2}$. (c) HMM presentation for the classical stochastic process resulting from measurement ($\theta = \pi/2$) of the quantum process generated by (b). (d) Mixed states for the stochastic process generated by (c) in that HMM's state distribution simplex. Each mixed state is a point of the form (p_A, p_B, p_C) with probabilities of being in state A, B, or C of (c). The color scale shows the logarithm of the probability of the mixed states.

$x \in \mathcal{A}$ are

$$T^{(x)} = \sum_{\rho_j} \mathbb{T}^{\rho_j} \Pr(x|\rho_j), \tag{4}$$

where $\Pr(x|\rho_j) = \mathrm{tr}(E_x \rho_j E_x^\dagger)$ and the cCQS labeled transition matrices $\mathbb{T}^{\rho_j}$ are defined in SM [30] Sec. II A. See the HMM in Fig. 2(c). It generates the classical process resulting from measuring the qubit process generated by Fig. 2(b) with angles $\phi = 0$ and $\theta = \pi/2$.

Uncountable predictive features. One would hope that, since here we know the measured cCQS, as shown in Fig. 2(c) for the example there, and it generates the measured qubit process, we could apply Eqs. (1) and (2) to calculate our measures of randomness and memory directly from that model. Unfortunately, a problem arises. The measured cCQS is not an ϵ-machine since the generated measurement sequences are not in one-to-one correspondence with the internal state sequences. This is the problem of measured-cCQS *nonunifilarity* and it stymies any attempt to directly calculate the randomness and memory of the measured quantum process. In fact, and this is the first part of our result, nonunifilarity is generic to measured cCQSs, since randomly sampled HMMs are nonunifilar [35].

Though Fig. 2(c)'s HMM generates the observed qubit process, we cannot use it to directly determine even the most basic process properties. Fortunately, this measured cCQS can be converted to an ϵ-machine by calculating the cCQS's *mixed states*; for details, see SM [30] Sec. II C. Here, we give a synopsis.

As first formalized by Blackwell [36], an N-state HMM's mixed states are conditional probability distributions $\eta(x_{-\ell:0}) = \Pr(\mathcal{R}_0 | X_{-\ell:0} = x_{-\ell:0})$ over the measured HMM's internal states $\mathcal{R}$ given all sequences $x_{-\ell:0} \in \mathcal{A}^\ell$. The collection over all of a process' allowed sequences induces a (Blackwell) measure μ on the state distribution $\Pr(\mathcal{R})$ ($N-1$)-dimensional simplex $\boldsymbol{\mathcal{R}}$. The mixed states together with the mixed-state transition dynamic give an HMM's *mixed-state presentation* (MSP).

A mixed state answers the question, given that one knows the HMM structure and has seen a particular sequence, what is the best guess of the internal state probabilities? Recurrent mixed states exactly correspond to causal states $\boldsymbol{\mathcal{S}}$ [37]. When they lay in an uncountable set $S \subseteq \boldsymbol{\mathcal{R}}$—see Fig. 2(d)—$C_\mu$ diverges.

Measurement-induced nonunifilarity results in the number of causal states diverging. That is, despite the controller having only a finite number of states and the controlling cCQS being unifilar, measurement means that predicting the observed process requires an uncountable number of causal states. This also introduces another fundamental challenge: how to define and quantify the resulting randomness and complexity.

Measurement-induced randomness and statistical complexity. The uncountable causal states also render the complexity measure expressions in Eqs. (1) and (2) unusable. Fortunately, Blackwell provided a formal expression for the entropy rate [36] by showing that an HMM's mixed-state presentation is unifilar. The entropy rate is then an integral over the invariant Blackwell measure $\mu(\eta)$ in the mixed-state simplex $\boldsymbol{\mathcal{R}}$,

$$h_\mu^B = -\int_{\boldsymbol{\mathcal{R}}} d\mu(\eta) \sum_{x \in \mathcal{A}} \Pr(x|\eta) \log_2 \Pr(x|\eta). \tag{5}$$

Recently, Ref. [38] introduced a constructive approach to evaluate this integral by establishing contractivity of the simplex maps—the substochastic transition matrices of Eq. (4)—and showing that the mixed-state process is ergodic. Given ergodicity of the mixed-state process, rather than integrate over the Blackwell measure $\mu(\eta)$, such as in Fig. 2(d), we can average over a time series of mixed states μ_t to get the measured cCQSs entropy rate,

$$\widehat{h_\mu^B} = -\lim_{\ell \to \infty} \frac{1}{\ell} \sum_{i=0}^{\ell} \sum_{x \in \mathcal{A}} \Pr(x|\eta_i) \log_2 \Pr(x|\eta_i), \tag{6}$$

where $\Pr(x|\eta_i) = \eta(x_{0:i}) \cdot T^{(x)} \cdot \mathbf{1}$, $x_{0:i}$ is the first i symbols of an arbitrarily long sequence $x_{0:\infty}$ generated by the process, and $\mathbf{1}$ is a column vector of all 1's.

Calculating the memory of the measured cCQS—the statistical complexity C_μ—is similarly delicate. In the typical case the causal state set $\boldsymbol{\mathcal{S}}$ of the measured cCQS is uncountable,

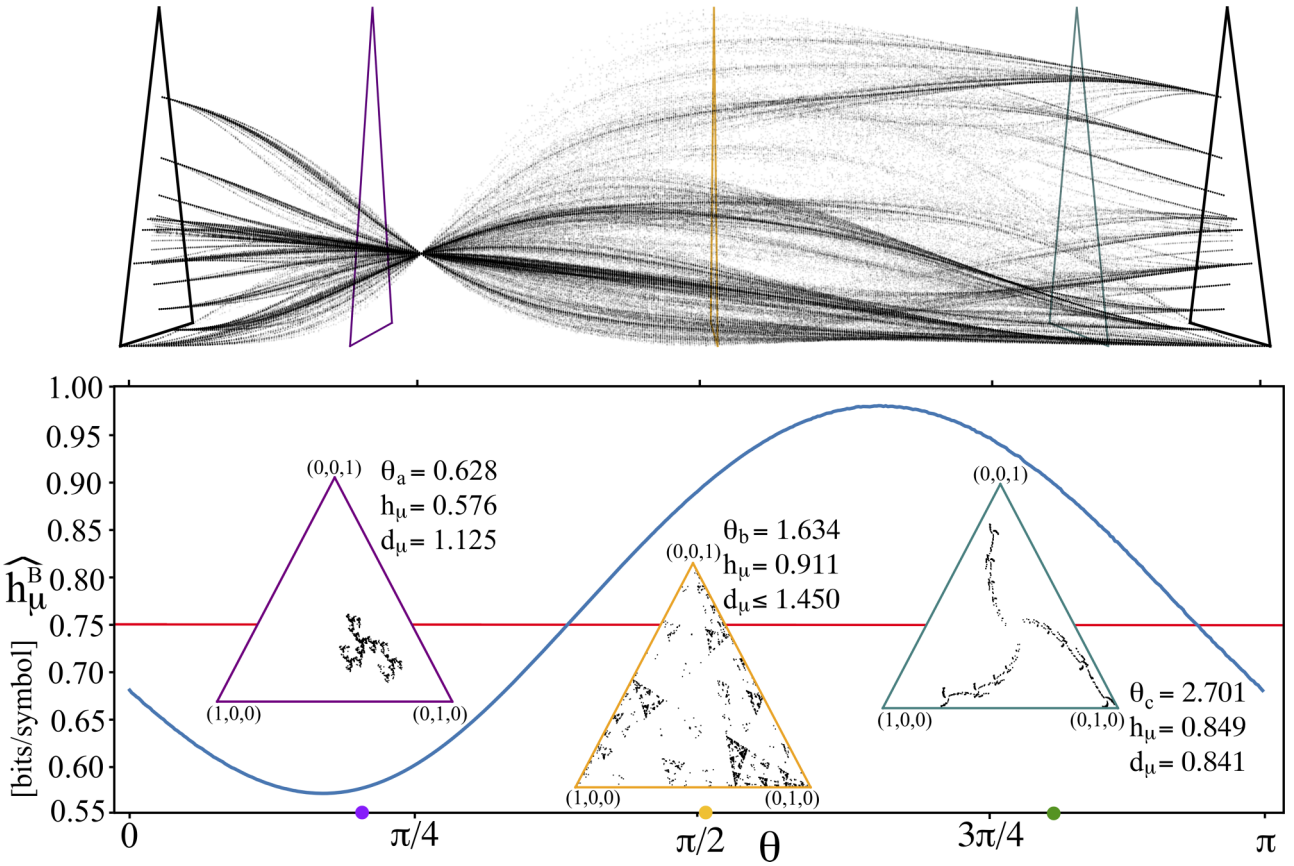

FIG. 3. Measurement-induced randomness and structure. Top: Mixed-state sets when measuring the qubit process of Fig. 2(b) as a function of measurement angle $\theta \in [0, \pi]$. Bottom: Entropy rate $\widehat{h}_\mu^B$ (blue curve) as a function of angle. The horizontal line (red) is the entropy rate of the (unmeasured) qubit sequences: $h_\mu^s = 3/4$ bit per output qubit. Insets: Mixed states at three measurement angles: (a) $\theta_a = 0.628$ (purple), (b) $\theta_b = 1.634$ (orange), and (c) $\theta_c = 2.701$ (green). The measured process entropy rates h_μ and statistical complexity dimensions d_μ given there. Both mixed states and complexity measures are computed with $\ell = 10^6$ iterates.

and C_μ diverges. Instead, we track its rate of divergence—the *statistical complexity dimension* d_μ of the Blackwell measure μ on $\boldsymbol{\mathcal{R}}$ [35,39],

$$d_\mu = \lim_{\epsilon \to 0} -\frac{\mathrm{H}_\epsilon[\mathcal{R}]}{\log_2 \epsilon}, \tag{7}$$

where $\mathrm{H}_\epsilon[Q]$ is the Shannon entropy (in bits) of the continuous-valued random variable Q, coarse-grained at size ϵ, and $\mathcal{R}$ is the random variable associated with the mixed states $\eta \in \boldsymbol{\mathcal{R}}$. SM [30] Secs. II C and II E develop an upper bound on d_μ that can be accurately determined from the measured process' entropy rate $\widehat{h}_\mu^B$ above and the mixed-state process' Lyapunov characteristic exponent spectrum Λ. As discussed in SM [30] Sec. II E and Ref. [39], this upper bound can be a close approximation to d_μ, but may also be a strict inequality.

Measurement dependence. Equations (3) and (4) indicate that the choice of measurement basis alters the observed process. To explore this with an example, we calculate the dependence of the above complexity measures as a function of measurement angle θ, with fixed ϕ for Fig. 2(b)'s cCQS, determining the measured cCQS at each measurement setting.

Figure 3 (top) shows the results. The cCQS is measured in 500 different bases, holding $\phi = 0$ fixed and varying $\theta \in [0, \pi]$ uniformly. For each measured cCQS the MSP is computed and the resulting series of mixed-state sets is plotted. Figure 3 (bottom) plots $\widehat{h}_\mu^B(\theta)$ and highlights three particular measurement angles $\{\theta_a, \theta_b, \theta_c\}$, showing the unique attractor found in the latter's mixed-state simplices. MSP entropy rate and the statistical complexity dimension are estimated using Eqs. (6) and (7), respectively.

Common characteristics are apparent, such as a smooth behavior of $h_\mu(\theta)$ with well-defined maxima and minima and the systematic change in the MSP structure as a function of θ which is consistent with the quoted dimensions d_μ. Angles $\theta = 0$ and $\theta = \pi$ give particularly simple behaviors with finite statistical complexity and $d_\mu = 0$, in accord with the countable MSPs there. The measured machines at these two values of θ are identical, aside from a symbol swap—all 0's become 1's and vice versa. They both have $C_\mu = 0.6813$ bits.

Figure 3 (top) exhibits a case of interest at $\theta = \pi/4$. The mixed states converge to a single point: a single-state machine that represents a biased coin. This occurs since the underlying cCQS has a binary quantum alphabet $\mathcal{A}_Q = \{\rho_0, \rho_+\}$ and the measurement basis corresponding to $\phi = 0$ and $\theta = \frac{\pi}{4}$ with basis vectors $|\psi_0\rangle$ and $|\psi_1\rangle$ is such that $\Pr(0|\rho_0) = \Pr(0|\rho_+)$ and $\Pr(1|\rho_0) = Pr(1|\rho_+)$. This basis is equidistant from both

quantum states in $\mathcal{A}_Q$. Therefore, applying the measurement to one state or the other yields the same probability distribution over outcomes. One loses all information about the underlying structure and the measured cCQS generates an *independent identically distributed* process.

To compare the randomness and organization of the underlying generator process, the horizontal line in the $\widehat{h}_\mu^B(\theta)$ plot gives the entropy rate of the (unmeasured) qubit process: $h_\mu^g = 3/4$ bit per output qubit. Its statistical complexity is $C_\mu^g = \mathrm{H}[\pi] = 1.5$ bits. The differences between these constant values and those of the measured cCQS values makes it clear that quantum measurement can both add or remove randomness and structure. A measurement close to $\theta = \frac{\pi}{4}$, on the one hand, rarely distinguishes between the measured quantum states ($|0\rangle\langle 0|$ or $|+\rangle\langle +|$) and has a greater number of measured 0's, making the measured process less random than the generating process. On the other hand, a measurement close to $\theta = 3\pi/4$ results in a more even distribution of measurement outcomes, introducing randomness to the measured process.

Conclusion. That randomness and complexity arise when observing qubit processes can be too facilely appreciated. Indeed, quantum measurement often comes steeped in mystery. We dispelled some of that mystery by showing that (i) an infinite number of predictive features are required to describe measured qubit time series and (ii) measurement can both introduce and subtract information and correlation. These characters of measurement greatly complicate learning about the informational and dynamical organization of quantum systems. However, at least now, we can appreciate more fully what the task is, what mechanism drives it (nonunifilarity), and why it is challenging.

Unexpectedly, analyzing the quantum physics necessitated another theory and efficient algorithms for quantifying the randomness and complexity of ergodic, stationary processes generated by nonunifilar hidden Markov models. Mathematically, these gave a constructive answer to the longstanding information-theoretic problem of characterizing functions of Markov chains—a problem that until now had only been formally, not constructively, solved [36].

Solving the problem of measurement-induced complexity is a step to fully describing quantum systems in terms of measurements. The results shed light on the fundamental ways in which the measurement act influences the observed complexity of quantum systems. With these tools, on the one hand, the next steps to reduce observed complexity easily come to mind: using positive operator-valued measures (POVMs), implementing multiqubit measurements, and developing adaptive measurement schemes. On the other hand, introducing quantum controllers will bring results that bear directly on contemporary experimental systems, such as single-photon sources.

Acknowledgments. We thank C. Aghamohammadi, F. Anza, S. Loomis, S. Marzen, and T. Pittman for helpful discussions. A.E.V.L., A.M.J., and J.P.C. thank the Santa Fe Institute and J.P.C. thanks the Telluride Science Research Center, Institute for Advanced Study at the University of Amsterdam, and California Institute of Technology for their hospitality during visits. This material is based upon work supported by, or in part by, the U.S. Army Research Laboratory and the U.S. Army Research Office under Contracts No. W911NF-13-1-0390 and No. W911NF-18-1-0028.

[1] E. Schrödinger, The present situation in quantum mechanics, Proc. Am. Philos. Soc. **124**, 323 (1935).

[2] C. S. Wu and I. Shaknov, The angular correlation of scattered annihilation radiation, Phys. Rev. **77**, 136 (1950).

[3] J. S. Bell, On the Einstein Podolsky Rosen paradox, Physics **1**, 195 (1964).

[4] A. Einstein, B. Podolsky, and N. Rosen, Can quantum-mechanical description of physical reality be considered complete? Phys. Rev. **47**, 777 (1935).

[5] A. K. Ekert, Quantum Cryptography Based on Bell's Theorem, Phys. Rev. Lett. **67**, 661 (1991).

[6] C. H. Bennett, G. Brassard, C. Crepeau, R. Jozsa, A. Peres, and W. K. Wootters, Teleporting an Unknown Quantum State via Dual Classical and Einstein-Podolsky-Rosen Channels, Phys. Rev. Lett. **70**, 1895 (1993).

[7] V. Giovannetti, S. Lloyd, and L. Maccone, Quantum Metrology, Phys. Rev. Lett. **96**, 010401 (2006).

[8] R. Raussendorf and H. J. Briegel, A One-Way Quantum Computer, Phys. Rev. Lett. **86**, 5188 (2001).

[9] M. Lindemann, G. Xu, T. Pusch, R. Michalzik, M. R. Hofmann, I. Zutic, and N. C. Gerhardt, Ultrafast spin-lasers, Nature (London) **568**, 212 (2019).

[10] S. J. Freedman and J. F. Clauser, Experimental Test of Local Hidden-Variable Theories, Phys. Rev. Lett. **28**, 938 (1972).

[11] R. Miller, T. E. Northup, K. M. Birnbaum, A. Boca, A. D. Boozer, and H. J. Kimble, Trapped atoms in cavity QED: Coupling quantized light and matter, J. Phys. B: At., Mol. Opt. Phys. **38**, S551 (2005).

[12] P. G. Kwiat, K. Mattle, H. Weinfurter, A. Zeilinger, A. V. Sergienko, and Y. Shih, New High-Intensity Source of Polarization-Entangled Photon Pairs, Phys. Rev. Lett. **75**, 4337 (1995).

[13] O. Benson, C. Santori, M. Pelton, and Y. Yamamoto, Regulated and Entangled Photons from a Single Quantum Dot, Phys. Rev. Lett. **84**, 2513 (2000).

[14] H. Walther, B. T. H. Varcoe, B.-G. Englert, and T. Becker, Cavity quantum electrodynamics, Rep. Prog. Phys. **69**, 1325 (2006).

[15] M. D. Eisaman, J. Fan, A. Migdall, and S. V. Polyakov, Single-photon sources and detectors, Rev. Sci. Instrum. **82**, 071101 (2011).

[16] F. A. Pollock, C. Rodriguez-Rosario, T. Frauenheim, M. Paternostro, and K. Modi, Non-Markovian quantum processes: Complete framework and efficient characterization, Phys. Rev. A **97**, 012127 (2018).

[17] M. A. Nielsen and I. L. Chuang, *Quantum Computation and Quantum Information*, 10th anniversary ed. (Cambridge University Press, Cambridge, UK, 2011).

[18] R. Rey de Castro, R. Cabrera, D. I. Bondar, and H. Rabitz, Time-resolved quantum process tomography using Hamiltonian-encoding and observable-decoding, New J. Phys. **15**, 025032 (2013).
[19] M. Holzäpfel, T. Baumgratz, M. Cramer, and M. B. Plenio, Scalable reconstruction of unitary processes and Hamiltonians, Phys. Rev. A **91**, 042129 (2015).
[20] C. Granade, J. Combes, and D. G. Cory, Practical Bayesian tomography, New J. Phys. **18**, 033024 (2016).
[21] M. Kliesch, R. Kueng, J. Eisert, and D. Gross, Guaranteed recovery of quantum process from few measurements, Quantum **3**, 171 (2019).
[22] A. M. Palmieri, E. Kovlakov, and F. Bianchi, Experimental neural network enhanced quantum tomography, npj Quantum Inf. **6**, 20 (2020).
[23] L. C. G. Govia, G. J. Ribeill, D. Riste, M. Ware, and H. Krovi, Bootstrapping quantum process tomography via perturbative ansatz, Nat. Commun. **11**, 1084 (2020).
[24] IBM quantum experience, https://quantum-computing.ibm.com.
[25] Rigetti cloud services, https://rigetti.com.
[26] J. P. Crutchfield and K. Young, Inferring Statistical Complexity, Phys. Rev. Lett. **63**, 105 (1989).
[27] J. P. Crutchfield, Between order and chaos, Nat. Phys. **8**, 17 (2012).
[28] C. Galland, Y. Ghosh, A. Steinbru, M. Sykora, J. A. Hollingsworth, V. I. Klimov, and H. Htoon, Two types of luminescence blinking revealed by spectroelectrochemistry of single quantum dots, Nature (London) **479**, 203 (2011).
[29] A. L. Efros and D. J. Nesbitt, Origin and control of blinking in quantum dots, Nat. Nanotechnol. **11**, 661 (2016).
[30] See Supplemental Material at http://link.aps.org/supplemental/10.1103/PhysRevE.102.040102 for a review of our quantum formalism, classical stochastic processes, information measures, mixed states, and details of the numerical calculations, which includes Refs. [40–53].
[31] L. R. Rabiner and B. H. Juang, An introduction to hidden Markov models, IEEE ASSP Mag. **3**, 4 (1986).
[32] L. R. Rabiner, A tutorial on hidden Markov models and selected applications, IEEE Proc. **77**, 257 (1989).
[33] J. Bechhoefer, Hidden Markov models for stochastic thermodynamics, New. J. Phys. **17**, 075003 (2015).
[34] C. E. Shannon, A mathematical theory of communication, Bell Sys. Tech. J. **27**, 379 (1948); **27**, 623 (1948).
[35] S. E. Marzen and J. P. Crutchfield, Nearly maximally predictive features and their dimensions, Phys. Rev. E **95**, 051301(R) (2017).
[36] D. Blackwell, The entropy of functions of finite-state Markov chains, in *Transactions of the First Prague Conference on Information Theory, Statistical Decision Functions, Random Processes* (Czechoslovak Academy of Sciences, Prague, 1957), Vol. 28, pp. 13–20.
[37] C. J. Ellison, J. R. Mahoney, and J. P. Crutchfield, Prediction, retrodiction, and the amount of information stored in the present, J. Stat. Phys. **136**, 1005 (2009).
[38] A. Jurgens and J. P. Crutchfield, Shannon entropy rate of hidden Markov processes, arXiv:2008.12886.
[39] A. Jurgens and J. P. Crutchfield, Infinite complexity of finite state hidden Markov processes, (unpublished).
[40] M. Gu, K. Wiesner, E. Rieper, and V. Vedral, Quantum mechanics can reduce the complexity of classical models, Nat. Commun. **3**, 762 (2012).
[41] J. R. Mahoney, C. Aghamohammadi, and J. P. Crutchfield, Occam's quantum strop: Synchronizing and compressing classical cryptic processes via a quantum channel, Sci. Rep. **6**, 20495 (2016).
[42] P. M. Riechers, J. R. Mahoney, C. Aghamohammadi, and J. P. Crutchfield, Minimized state-complexity of quantum-encoded cryptic processes, Phys. Rev. A **93**, 052317 (2016).
[43] C. Aghamohammadi, J. R. Mahoney, and J. P. Crutchfield, The ambiguity of simplicity, Phys. Lett. A **381**, 1223 (2017).
[44] S. Loomis and J. P. Crutchfield, Strong and weak optimizations in classical and quantum models of stochastic processes, J. Stat. Phys. **176**, 1317 (2019).
[45] T. M. Cover and J. A. Thomas, *Elements of Information Theory* (Wiley-Interscience, New York, 1991).
[46] J. P. Crutchfield and D. P. Feldman, Regularities unseen, randomness observed: Levels of entropy convergence, Chaos **13**, 25 (2003).
[47] R. G. James, C. J. Ellison, and J. P. Crutchfield, Anatomy of a bit: Information in a time series observation, Chaos **21**, 037109 (2011).
[48] P. Frederickson, J. Kaplan, E. Yorke, and J. Yorke, The Lyapunov dimension of strange attractors, J. Differ. Equations **49**, 185 (1983).
[49] J. Kaplan and J. Yorke, Chaotic behavior of multidimensional difference equations, in *Functional Differential Equations and Approximation of Fixed Points*, Lecture Notes in Mathematics Vol. 730 (Springer, Berlin, 1979), pp. 204–227.
[50] D. Feng and H. Hu, Dimension theory of iterated function systems, Commun. Pure Appl. Math. **62**, 1435 (2009).
[51] A. Jurgens and J. P. Crutchfield, Backwards entropy rate of hidden Markov processes, in preparation 2020 (unpublished).
[52] A. Jurgens and J. P. Crutchfield, Minimal embedding dimension of minimally infinite hidden Markov processes, (unpublished).
[53] K. Falconer, *Fractal Geometry: Mathematical Foundations and Applications* (Wiley, Chichester, 1990).